Novel geomagnetic field morphological criteria: from Modern to Pleistocene eras

Filipe Terra-Nova[1,*], Ingo Wardinski[2], Sanja Panovska[3], Monika Korte[3]

[1] *Nantes Université, Univ Angers, Le Mans Université, CNRS, Laboratoire de Planétologie et Géosciences, LPG UMR 6112, 44000 Nantes, France.*

[2] *Institut Terre et Environnement Strasbourg, Ecole et Observatoire des Sciences de La Terre, Université de Strasbourg, CNRS UMR 7063, Strasbourg, France.*

[3] *GFZ German Research Centre for Geosciences, Section 2.3, Helmholtz Centre Potsdam, Potsdam, Germany.*

Abstract

We evaluate the morphological characteristics of the geomagnetic field in 22 models that span distinctive timescales. We consider classical criteria that were used to quantify the Earth likeness of numerical dynamo simulations[1] as well as new quantities that correspond to the presence of regions of weak field, including surface intensity minima and polar minima on the core-mantle boundary, and criteria that quantify the impact of mantle control on Earth's magnetic field, including the existence of pairs of high-latitude intense flux patches at each hemisphere and a polar minima North-South magnitude dichotomy.

Methods

CLASSICAL CRITERIA Recalling the four morphological criteria[1] to evaluate the Earth likeness of numerical dynamo models:

- AD/NAD: ratio of the power of the axial dipole to the power of the rest of the field.
- O/E: ratio of the power in equatorially anti-symmetric non-dipole to the power in equatorially symmetric non-dipole components.
- Z/NZ: ratio of the power in the non-dipole zonal to the non-dipole non-zonal field.
- FCF: flux concentration evaluated by the variance of B_r^2.

NOVEL CRITERIA

Weak field

- Minimum field intensity at Earth's surface F_{min} relative to its mean value $\langle F \rangle$

$$F^*_{min} = \frac{F_{min}}{\langle F \rangle} \tag{1}$$

For a pure axial dipole field $F^*_{min} \approx 0.725$.

- Magnitude of geomagnetic polar minima at the CMB[2]:

$$\mathrm{PM} = \begin{cases} \dfrac{|B_r^{NP} - min(B_r)|}{max|B_r^z|}, & \text{in the Northern Hemisphere} \\ \dfrac{|B_r^{SP} - max(B_r)|}{max|B_r^z|}, & \text{in the Southern Hemisphere} \end{cases} \tag{2}$$

where B_r^{NP} and B_r^{SP} are the radial field at the North and South Poles, respectively, and B_r^z is the zonal radial field. The mean magnitude of the two polar minima:

$$\mathrm{PMM} = \frac{\mathrm{PM_{NH}} + \mathrm{PM_{SH}}}{2} \tag{3}$$

For a pure dipole field with a tilt of $\theta_{dip} = 20.43°$ (maximum tilt in the GFF100k model), PM is ≈ 0.067. The existence of polar minima is considered for PMM > 0.067.

Mantle control on the geomagnetic field

- Because lower mantle seismic models have a dominant degree and order 2 pattern[3], a typical mantle controlled magnetic field is defined by the presence of equatorially anti-symmetric pairs of high-latitude intense flux patches (Flux Patch Duet, FPD). Applying a Fast Fourier Transform to the latitudinal average of B_r^2 at the CMB[3], FPD is defined based on the resulting amplitudes of the complex Fourier functions:

$$\mathrm{FPD} = \frac{A_2}{(A_1 + A_3 + ... + A_{\ell_{max}})/(\ell_{max} - 1)} \tag{4}$$

For an equipartitioned field the latitudinal averaged B_r^2 is flat and FPD is unity.

- The difference in the magnitudes of the two polar minima

$$\mathrm{PMD} = \mathrm{PM_{NH}} - \mathrm{PM_{SH}}. \tag{5}$$

Stronger polar minima in the Northern/Southern hemisphere give positive/negative PMD values, respectively. PMD approaches zero for small differences between the two.

Results

Geomagnetic field models, their setup and the time intervals analyzed.

Model (Reference)	ℓ_{max}	Data	Era	Time interval
CHAOS7.13 (Finlay et al., 2020)	22	St,O	Mod	1997 AD-2022 AD
KALMAG (Baerenzung et al., 2022)	14	St,O,H	Hist	1900 AD-2016 AD
GUFM1 (Jackson et al., 2000)	14	O,H	Hist	1840 AD-1990 AD
COV-OBS.x1 (Gillet et al., 2015)	14	St,O,H	Hist	1840 AD-2018 AD
BIGMUDIh.1 (Arneitz et al., 2021)	14	O,H	Hist	1380 AD-1920 AD
SHAWQ2k (Campuzano et al., 2019)	10	A,L	Arch	0000 AD-1900 AD
ARCH3k (Korte et al., 2019)	14	A,L	Arch	1000 BC-1900 AD
A_FM-M (Licht et al., 2013)	5	A,L	Arch	1000 BC-1900 AD
ASD_FM-M (Licht et al., 2013)	5	A,L,S	Arch	1000 BC-1900 AD
ASDI_FM-M (Licht et al., (2013)	5	A,L,S	Arch	1000 BC-1900 AD
COV-ARCH (Helio and Gillet,2018)	10	A,L	Arch	1000 BC-1850 AD
COV-LAKE (Helio and Gillet, 2018)	10	A,L,S	Arch	1000 BC-1850 AD
BIGMUDI4k (Arneitz et al., 2019)	8	H,A,L	Arch	1000 BC-1900 AD
SHA.DIF.14k (Pavón-Carrasco et al., 2014)	10	A,L	Holo	5000 BC-1800 AD
ArchKalMag14k (Schanner et al., 2022)	20	A,L	Holo	6000 BC-1900 AD
pfm9k.2 (Nilsson et al., 2022)	8	A,L,S	Holo	7000 BC-1950 AD
HFM10k.ALO.1 (Constable et al., 2016)	10	A,L,S	Holo	8000 BC-1900 AD
CALS10K.2 (Constable et al., 2016)	10	A,L,S	Holo	8000 BC-1900 AD
LSMOD.2 (Korte et al., 2019)	10	A,L,S	Pleis	40k BC-28k BC
GGFS70k (Panovska et al., 2021)	6	S	Pleis	70k BC-14k AD
GGF100k (Panovska et al., 2018)	8	A,L,S	Pleis	100k BC-1650 BC
GGFMB (Magoub et al., 2023)	5	S	Pleis	900K BC-700k BC

Data type abbreviations stand for Archeomagnetic artifacts, Lava flows, Sediments, Historical navigation data, Observatories data and Satellite data. Time interval denotes the one used here.

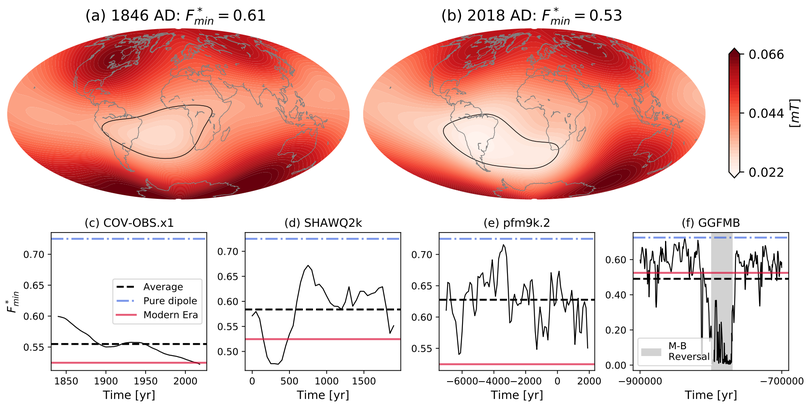

Fig.3 (a) and (b): Surface intensity for COV-OBS.x1 in 1860 AD and 2018 AD, respectively. Black contours denote surface intensity of 1.2 the minimum value. From (c) to (f): F^*_{min} as a function of time for a Historical (c), an Archeological (d), a Holocene (e) and a Pleistocene (f) field models. In (a) and (b) the models are expanded until $\ell_{max} = 13$, in (c)-(f) $\ell_{max} = 5$.

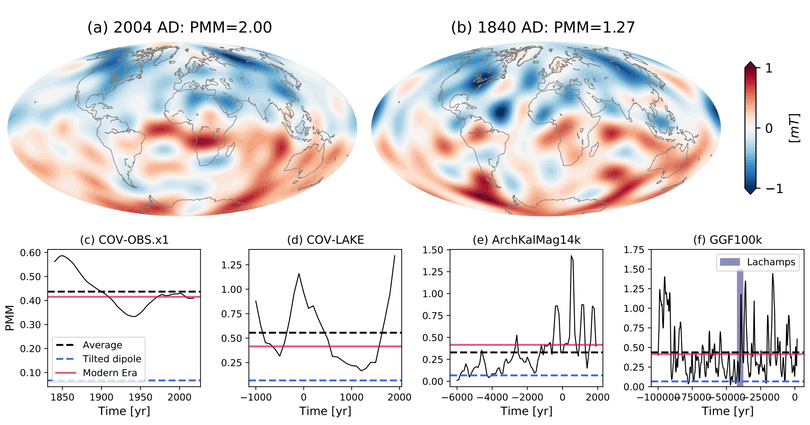

Fig.4 (a) and (b): Radial field at the CMB for COV-OBS.x1 in 2004 AD and 1840 AD, respectively. (a) and (b) are maximum and minimum of PMM for COV-OBS.x1, respectively.

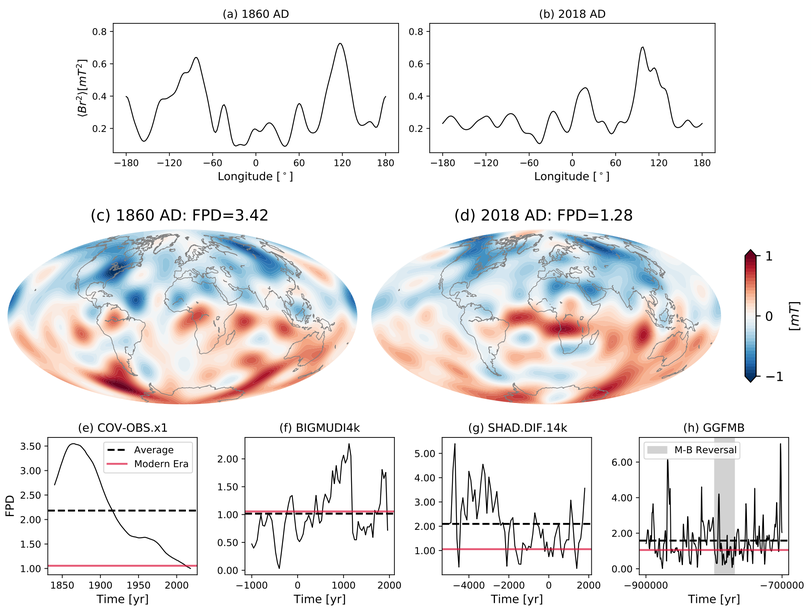

Fig.5 (a) and (b): B_r^2 averaged along longitude lines at the CMB. (c) and (d): radial field at the CMB.

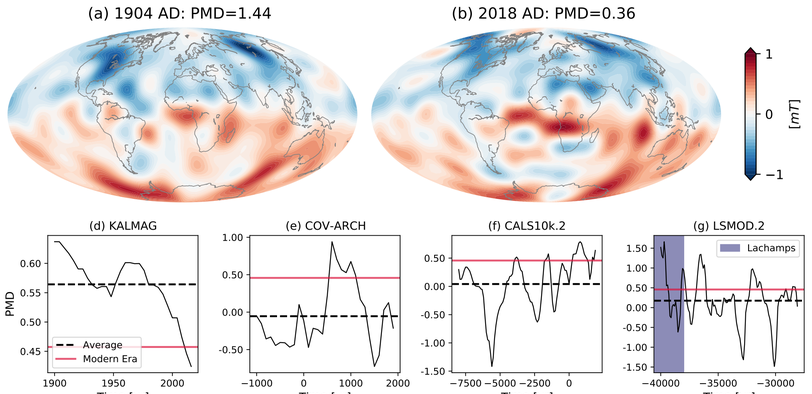

Fig. 6 As in Fig. 4 for PMD.

NEW BOUNDS FOR EARTH LIKENESS Target values Π_i^E based on the mean of the time-averaged values of all models grouped by their assigned era and the allowed bounds determined by the assigned standard deviations σ_i^E of the criteria.

	AD/NAD	O/E	Z/NZ	FCF	F^*_{min}	PMM	FPD	PMD
From[1]								
Π_i^E	1.40	1.00	0.15	1.50	-	-	-	-
Modern era truncated at $\ell_{max} = 8$								
Π_i^E	0.94	0.84	0.33	1.40	0.49	1.15	1.53	1.31
Modern era truncated at $\ell_{max} = 5$								
Π_i^E	1.30	0.88	0.35	1.03	0.52	0.42	1.06	0.46
Historical era								
Π_i^E	1.86	0.82	0.32	1.19	0.56	0.41	1.73	0.52
Archeological era								
Π_i^E	2.83	0.87	0.24	1.26	0.59	0.39	1.50	0.07
Holocene era								
Π_i^E	4.01	1.03	0.23	1.38	0.61	0.40	1.78	0.17
Pleistocene era								
Π_i^E	1.80	0.91	0.28	1.93	0.49	0.59	1.60	0.12
All eras								
σ_i^E	2.00[a]	2.00[a]	2.50[a]	1.75[a]	1.40	2.00	2.00	1.55

[a] from[1]. Π_i^E is the target value and σ_i^E represents how much the value can depart from its mean to score well.

Spatial resolution dependence

- Both classical and new criteria strongly depend on the models spatial resolution.
- Five out of the eight criteria have significantly larger variations from truncation at spherical harmonic degree $\ell_{max} = 5$ to $\ell_{max} = 6$ compared to differences between other pairs of successive ℓ_{max} values.

CLASSICAL CRITERIA

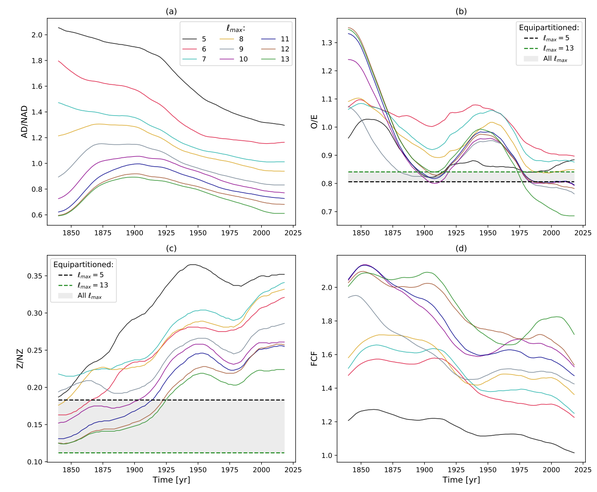

Fig. 1 The dependence of the four classical morphological criteria on the spatial truncation ℓ_{max} (colors) and time.

NOVEL CRITERIA

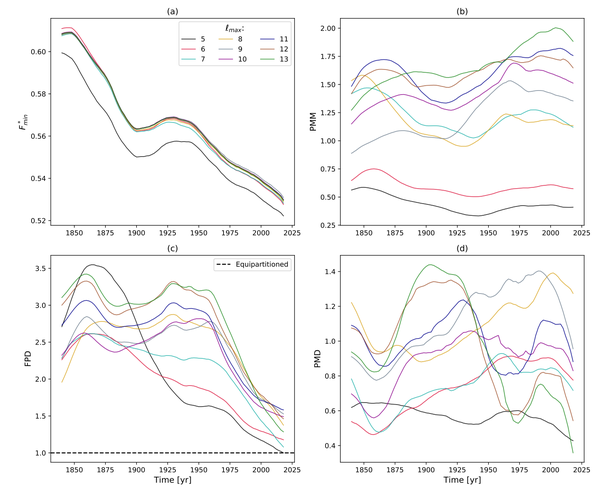

Fig. 2 As is Fig. 1 for the new morphological criteria.

Rating of compliance with present-day

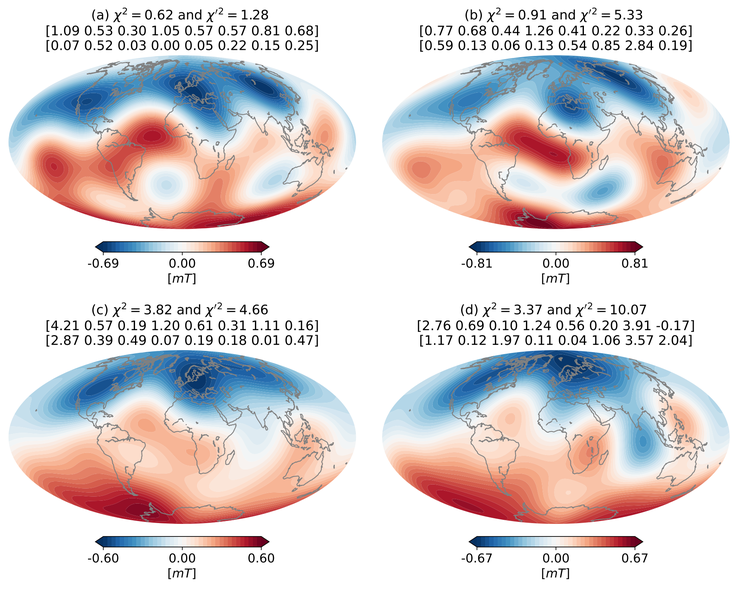

Fig. 7 Maps of the radial magnetic field at the CMB in 1000 AD of (a) COV-ARCH, (b) COV-LAKE, (c) HFM10k.ALO.1 and (d) ASDI_FM geomagnetic field models. The morphological criteria values AD/NAD, O/E, Z/NZ, FCF, F^*_{min}, PMM, FPD and PMD as well as their respective scores χ_i^2 are given above each map.

Discussion

- The well-known **decay of the geomagnetic axial dipole** and the **simultaneous increase in the non-dipole** field led to a decrease in AD/NAD since $\approx$ 1900 AD to present. However, for $\ell_{max} \geq 8$, AD/NAD increases between 1840-1900 due to a slower axial dipole decrease and a decrease in NAD with time.
- Presently, main zonal features are same-sign positive equatorial flux patches and the large region of **reversed flux below the Atlantic**. The latter and the **weakened high-latitude flux patch in the southern tip of South America break the anti-symmetry** of the present-day field[4].
- **Ancient field models that rely on sedimentary data**, which are poorly geographically distributed, produce **highly concentrated** fields at the CMB.
- All field models present **significant polar minima** suggesting **weak (or no) stratification** at the top of Earth's core[5].
- The radial geomagnetic field on the CMB is dominated by **pairs of equatorially symmetric intense high-latitude flux patches** more often than not, providing evidence for long-term **mantle control on the geodynamo**.
- The **new bounds** on the criteria can be used to **constrain numerical dynamo simulations** that aim to recover the pattern of the field.
- The overall **low compliance** of ancient field models with the modern field may suggest a **highly time-dependent geodynamo**.

References

[1] Christensen, U. R., Aubert, J., Hulot, G., 2010. Conditions for Earth-like geodynamo models. Earth Planet. Sci. Lett. 296, 487–496.

[2] Lézin, M., Amit, H., Terra-Nova, F., Wardinski, I., 2023. Mantle-driven north-south dichotomy in geomagnetic polar minima. Phys. Earth Planet. Inter. 337, 107000.

[3] Gubbins, D., 2003. Thermal core-mantle interactions: theory and observations. In: Dehant, V., Creager, K., Karato, S., Zatman, S. (Eds.), Earth's Core: dynamics, structure and rotation. AGU Geodynamics Series - American Geophysical Union.

[4] Finlay, C. C., Aubert, J., Gillet, N., 2016. Gyre-driven decay of the Earth's magnetic dipole. Nat. Commum. 7:10422.

[5] Olson, P., Landeau, M., Reynolds, E., 2017. Dynamo tests for stratification below the core-mantle boundary. Phys. Earth Planet. Inter. 271, 1–18.